First record of early Aptian Oceanic Anoxic Event 1a from the Paris Basin (France) - Climate signals on a terrigenous shelf

Jean-François Deconinck, Danny Boué, Francis Amédro, François Baudin, Ludovic Bruneau, Emilia Huret, Philippe Landrein, Jean-David Moreau, Anne Lise Santoni

First record of early Aptian Oceanic Anoxic Event 1a from the Paris Basin (France) - climate signals on a terrigenous shelf

Jean-François Deconinck[1], Danny Boué[1], Francis Amédro[1,2], François Baudin[3], Ludovic Bruneau[1], Emilia Huret[4], Philippe Landrein[4], Jean-David Moreau[1] and Anne Lise Santoni[1]

[1] Biogéosciences, UMR 6282, uB/CNRS, Université de Bourgogne/Franche-Comté, 6 Boulevard Gabriel, 21000 Dijon, France.

[2] 26 rue de Nottingham, 62100 Calais, France.

[3] ISTeP, UMR 7193, SU/CNRS, Sorbonne Université, 4 Place Jussieu, 75005 Paris, France.

[4] Agence Nationale pour la gestion des déchets radioactifs, Centre de Meuse/Haute-Marne, RD 960, 55290 Bure, France.

Abstract

In 2013, Andra (French National Radioactive Waste Management Agency) drilled boreholes to the south-east of the Paris Basin, to characterise Aptian and Albian clayey formations, including the 'Argiles à Plicatules' Formation dated as early Aptian. One of these boreholes intersected this formation with an excellent recovery allowing detailed biostratigraphy (ammonites), sedimentology, clay mineralogy, isotope geochemistry ($\delta^{13}C_{org}$) and Rock-Eval analyses to be performed. The base of the formation corresponds to transgressive dark-grey silty clays with iron oolites and plant debris indicating a coastal environment evolving up-section to upper offshore environments. Higher in the succession, clays with less than 4% $CaCO_3$ and less than 0.8% of organic matter were deposited in lower offshore environments. The occurrence of ammonites can be used to draw a biostratigraphic scheme, and in particular, to recognise the *deshayesi* and *furcata* ammonite Zones.

The clay mineral assemblages are composed of illite and kaolinite associated with minor amounts of chlorite, vermiculite and smectite. The $\delta^{13}C_{org}$ values range between -24 and -25‰ except in a particular interval characterised by a prominent negative excursion of about -3‰, that is recognised worldwide and precedes Oceanic Anoxic Event 1a (OAE1a). This interval is also characterised by an abundance of kaolinite and the absence of smectite suggesting an acceleration of the hydrological cycle and enhanced runoff and hydrolysing conditions over the emerged landmasses just before and during the onset of OAE1a. This climate change is consistent with isotope and palynological data indicating warm and humid climate conditions before and during the onset of OAE1a. Surprisingly, the interval corresponding to OAE1a is not significantly enriched in organic matter and its lithology is not different from the rest of the core suggesting that Tethyan anoxic water masses did not reach the relatively shallow epicontinental environments of the Paris Basin.

Keywords: Lower Cretaceous, Aptian, Oceanic Anoxic Event, Paris Basin, Clay minerals, Organic carbon isotopes

Introduction

Identified for the first time by Schlanger and Jenkyns (1976), Oceanic Anoxic Event (OAE) 1a (early Aptian) is characterised by the worldwide preservation of organic matter in black shales as a consequence of intensification in marine primary productivity under oceanic oxygen-depleted conditions (Coccioni et al., 1987; 1992; Erba, 1994, Erba, 2004; Erbacher et al., 1996; Leckie et al., 2002; Jenkyns, 2010; Föllmi, 2012; Erba et al., 2015). A global perturbation in the carbon cycle is associated with this event, recorded by a prominent negative excursion followed by a shift towards more positive values (Menegatti et al., 1998).

The negative excursion is generally explained by an intense volcanic episode at the origin of the formation of the Ontong-Java oceanic plateau (Tarduno et al., 1991; Larson and Erba, 1999; Méhay et al., 2009; Tejada et al., 2009; Bottini et al., 2012; Erba et al., 2015; Charbonnier and Föllmi, 2017) while the following positive excursion is seen as a consequence of organic matter burial in oceanic sediments. The duration of the negative excursion, first underestimated between 27 and 44 kyr (Li et al., 2008), is likely longer with a duration estimated between 280 and 350 kyr (Lorenzen et al., 2013). The duration of OAE1a itself is estimated between 1 and 1.3 myr (Li et al., 2008). These environmental changes were associated with rising sea surface temperatures (Mutterlose et al., 2014; Bottini et al., 2015) and a calcification crisis in calcareous nannoplankton known as the 'nannoconid crisis' (Erba, 1994). Despite its widespread extension and its recognition in numerous sedimentary basins (Bréhéret, 1997; Bellanca et al., 2002; Ando et al., 2008; Vincent et al., 2010; Giraud et al., 2018 among others) and shallow water carbonate platforms (Baudin et al., 1996; Luciani et al., 2006; Najarro et al., 2011; Graziano, 2013; Godet et al., 2014; Pictet et al., 2015; Amodio and Weissert, 2017; Hueter et al., 2019), OAE1a has not yet been described in the Paris Basin mainly because lower Aptian clayey deposits are poorly outcropping. In 2013, several boreholes were drilled by Andra (the French National Radioactive Waste Management Agency) to the south-east of the Paris Basin in order to characterise Aptian and Albian clayey formations including Argiles à Plicatules, a so-called formation because of the occasional occurrence of *Plicatula placunea* Lamarck, 1819, a common warm water bivalve (Squires and Saul, 1997). One of these boreholes (AUB 121) intersected the Argiles à Plicatules Formation with excellent recovery allowing detailed sedimentological, mineralogical and geochemical studies to be performed; it also provided an opportunity to search for a record of OAE1a in the Paris Basin. As a result, facies descriptions as well as mineralogical, Rock-Eval and $\delta^{13}C_{org}$ analyses were performed to characterise the Aptian sediments deposited in the Paris

Basin. The main objectives were to precisely describe the whole succession of the Argiles à Plicatules Formation, to highlight the record of OAE1a in the terrigenous shelf environment of the Paris Basin and to specify climatic conditions, notably the fluctuations in the hydrological cycle that prevailed during the Aptian through a high resolution study of the clay minerals.

I - Geological context and biostratigraphy

The Paris Basin is a Meso-Cenozoic intracontinental basin that, today, is bordered by Palaeozoic massifs including the Armorican Massif to the west, the Massif Central to the south, the Vosges to the east and the Ardennes Massif to the north. During the Aptian, the Paris Basin was occupied by a narrow epicontinental sea (strait) between the London-Brabant Massif (LBM) and the Rhenish Massif (RM) to the north and a landmass comprising the Armorican Massif (AM) and the Massif Central (MC) to the south (Fig. 1). This narrow epicontinental sea, situated at a latitude comprised between 30 and 35°N, connected the Tethys Ocean located to the south-east to the boreal realm toward the north-west (Masse et al., 2000).

After a long period of continental evolution of the Paris Basin starting at the Jurassic/Cretaceous transition (Purbeckian facies), transgressive marine sediments were deposited above Early Cretaceous variegated continental and deltaic sediments, the so-called Wealden facies (Allen, 1998; Guillocheau et al., 2000; Radley and Allen, 2012). To the south-east of the Paris Basin, the Early Cretaceous continental sedimentation (Berriasian to Barremian) was occasionally interrupted by the deposition of shallow marine sediments including the early Hauterivian "Calcaires à Spatangues" Formation and the early Barremian "Argiles Ostréennes" Formation, as a consequence of transgressions originating from the south-east (Tethyan domain), whereas the late Barremian continental deposits consist of

variegated clays showing common root traces. From the Aptian, a continuous marine sedimentation took place until the end of the Cretaceous.

I-1. Lithology of the AUB 121 borehole

The AUB 121 borehole is situated to the south-east of the Paris Basin, at Juzanvigny, near Brienne le Château (Fig. 2). The lithological succession has been described in detail by Amédro et al. (2017). The 31 m-thick Argiles à Plicatules Formation is underlain by upper Barremian continental deposits (Wealden facies) corresponding to weathering profiles (laterite) and overlain by upper Aptian glauconitic sands corresponding to the "Sables Verts de l'Aube" Formation (Fig. 3). Three distinct intervals (1 to 3) were defined within the Argiles à Plicatules Formation:

- Unit 1, from 116.76 m to 111.90 m, includes black to grey clays with traces of palaeosoils at the base. Woody debris and coalified compressions of pteridophytes are common in this part of the formation (Fig. 4A). Some iron oolites-rich layers (Fig. 4B) occasionally filling burrows occur at the base of this unit, while the top is marked by the presence of prominent shelly beds (between 112.40 m and 111.90 m) (Fig. 4C).
- Unit 2, from 111.90 m to 106.30 m, consists of a grey-brown bioturbated (*Chondrites*) clay, which appears to be homogeneous (no cycles can be distinguished). Some *Plicatula* occur occasionally and ammonites are common in the upper part of this unit.
- Unit 3, from 106.30 m to 86.10 m, corresponds to bioturbated khaki clays (*Chondrites*) in which the cycles are clearly individualised and limited at the base by bioturbated surfaces likely corresponding to firmgrounds. This poorly fossiliferous unit shows scattered *Plicatula*, some oysters and ammonites which

allow a biostratigraphic division to be esdetablished. Coarser quartz grains and glauconite occur at the topmost part of the formation announcing the overlying sandy glauconitic sedimentation (Sables Verts de l'Aube Formation).

I-2. Biostratigraphy

Ammonites have been systematically collected along the core (Fig. 3). Although they are not abundant, their study provides valuable information. A total of 19 ammonites were found in the 30.66 m of the Argiles à Plicatules Formation recovered in borehole AUB 121, of which 15 could be determined, at least at the generic level. They occur mostly as imprints in clays, and in a few cases as internal moulds preserved either in the form of pyritic nuclei or calcium phosphate nodules (Amédro et al., 2017). All recognised taxa are cosmopolitan, with a geographic distribution that includes the boreal, Tethyan and sometimes even southern realms. This wide geographic distribution is explained by the fact that the summit of the early Aptian corresponds to a high sea level (transgression of a second order eustatic cycle, see Jacquin et al., 1998). The vertical distribution of the ammonites permits to establish a biostratigraphic scheme.

The lower three meters of the Argiles à Plicatules Formation did not provide determinable ammonites in the Juzanvigny boreholes and therefore the stratigraphic attribution of the lowermost part of this formation remains uncertain. The occurrence of several *Roloboceras transiens* Casey, 1961 in the neighbouring department of Yonne and *Megatyloceras* at the base of the Argiles à Plicatules Formation (unpublished data) suggests that the interval could be attributed to the *Deshayesites forbesi* Zone, as these ammonites are characteristic of this biozone. The *Deshayesites deshayesi* Zone is undoubtedly recognised from 113.70 m to 105.15 m by the presence of an association including *Aconoceras (Aconoceras) nisoides* Sarasin, 1893, *Pseudosaynella bicurvata* Michelin, 1838, *Deshayesites deshayesi* d'Orbigny,

1841 and *Lithancylus grandis* J. de C. Sowerby, 1828. The *Dufrenoya furcata* Zone sensu Reboulet compiler (2018) [= the *Tropaeum bowerbanki* Zone described by Casey (1961)] is clearly identified from 102.50 m to 90.60 m by the occurrence of *Dufrenoyia* cf. *formosa* Casey, 1964 and *Dufrenoyia* cf. *furcata* J. de C. Sowerby, 1836.

II – Analytical methods

II–1. Carbon stable isotopes, Total Organic Carbon and calcimetry

Organic carbon isotope compositions ($\delta^{13}C_{org}$) and Total Organic Carbon (TOC) were measured on carbonate-free residues of 80 samples at the Biogéosciences Laboratory, Université Bourgogne/Franche-Comté in Dijon. Sample powders were reacted with HCl (2N) at room temperature for 24 h to remove the carbonate phases. Residues were rinsed with deionised distilled water until neutral, centrifuged (4500 rpm for 15 min), and then dried at 50°C overnight. Aliquots of dried decarbonated samples (~7–50 mg) were then weighed in tin capsules. TOC content and $\delta^{13}C_{org}$ measurements were performed at the Biogéosciences Laboratory of the University of Bourgogne/Franche-Comté (Dijon, France) on a Vario MICRO cube elemental analyzer (Elementar, Hanau, Germany) coupled in continuous flow mode to an IsoPrime stable isotope ratio mass spectrometer (Isoprime, Manchester, UK). USGS40 L-Glutamic acid (C = 40.8 wt%; $\delta^{13}C_{VPDB}$ = -26.39 ± 0.04‰) and IAEA-600 Caffeine ($\delta^{13}C_{VPDB}$ = -27.77 ± 0.04‰) certified reference materials were used for calibration. The carbon isotopic composition is expressed in delta notation and reported in per mil (‰) relative to the Vienna Pee Dee Belemnite (V-PDB) standard; the external reproducibility based on duplicate analyses of the samples is better than ± 0.2‰ (1σ).

The proportion of $CaCO_3$ is deduced by the difference in weight before and after decarbonation.

176 II–2. Organic matter characterisation

177 A Rock–Eval 6 Turbo apparatus (Vinci Technologies) was used for the quantitative
178 and qualitative study of organic matter from 34 selected samples distributed over the entire
179 section. The method, described in detail by Lafargue et al. (1998) and Behar et al. (2001),
180 consists of a two-step analysis with programmed temperature: pyrolysis, under inert
181 atmosphere (N_2), followed by oxidation. Samples were analysed at the Institut des Sciences de
182 la Terre de Paris (UMR7193/Sorbonne Université). Crushed samples are first subjected to a 3
183 min isotherm at 300°C at which free hydrocarbons are volatilised (peak S1). Then, a heating
184 step with a ramp rate of 25°C/min leads to the vaporisation of products via the thermal
185 cracking of organic matter up to 650°C (peak S2). Pyrolysis effluents are continuously
186 detected by a flame ionisation detector (FID) and expressed in mg per g of sample. Organic
187 CO and CO_2 are measured online as well by an infrared cell (peak S3). At the end of the
188 pyrolysis step, samples are automatically transferred into an oxidation oven where they are
189 subjected to a 1 min isotherm at 300°C then a ramp rate of 20°C/min up to 850°C. The total
190 signals of both organic and mineral CO and CO_2 are expressed in mg per g of samples. All
191 these parameters can be used to calculate the TOC content. The hydrogen index (HI),
192 corresponding to the quantity of hydrocarbon compounds released during pyrolysis relative to
193 the TOC (S2/TOC) in mg of HC per g of TOC as well as the oxygen index (OI)
194 corresponding to the organic CO_2 released during pyrolysis relative to the TOC (S3/TOC) in
195 mg of CO_2 per g of TOC are also calculated. HI and OI are correlated to the H/C and O/C
196 atomic ratios respectively, which can be used to determine the origin of the organic matter.
197 T_{max} is defined as the pyrolysis temperature at which the maximum amount of hydrocarbon is
198 yielded by kerogen (Espitalié et al., 1977). T_{max} increases linearly with the maturation degree
199 of the organic matter, thus giving a rapid estimate of the thermal maturity of sedimentary
200 basins (Espitalié, 1986).

II-3. Clay mineralogy

A total of 80 samples were analysed using X-Ray Diffraction (XRD). After moderate grinding in a mortar, powdered samples were decarbonated with a 0.2N HCl solution. The < 2 µm fraction (clay-sized particles) was extracted with a syringe after deflocculation and decantation of the suspension for 95 minutes following Stokes' law; this fraction was then centrifuged. Clay residue was then smeared on oriented glass slides and run in a Bruker D8 diffractometer with CuK_α radiations, a LynxEye detector and a Ni filter with a voltage of 40 kV and an intensity of 25 mA (Biogéosciences laboratory, Université Bourgogne/Franche-Comté in Dijon, France). Goniometer scanning ranged from 2.5° to 28° for each analysis. Three runs were performed for each sample to discriminate the clay phases: 1) air-drying; 2) ethylene-glycol solvation at room temperature during 24 hours; and 3) heating at 490°C during 2 hours, as recommended by Moore and Reynolds (1997). Clay minerals were identified using their main diffraction (d_{00l}) peaks and by comparing the three diffractograms obtained. The relative proportions of the clay minerals are estimated using peak intensity ratios. The error margin of the method is approximately ± 5 %.

III – Results

III-1. $CaCO_3$, Organic matter characterisation and $\delta^{13}C_{org}$

In the Argiles à Plicatules Formation, the proportion of $CaCO_3$ is very low (around 3%) in all of the samples studied (Fig. 5). The total organic carbon (TOC) content measured on the 34 selected samples using Rock-Eval pyrolysis is also very low, comprised between 0.1 and 0.52% (Table 1). As the quantity of organic matter (OM) is low, the Rock-Eval parameters are only partly reliable. However, some reliable T_{max} values lower than 420°C indicate that OM is immature (below the oil window). Organic matter is more abundant in

lithological unit 1 at the base of the section; this was expected since macroscopic woody debris and fern pinnules preserved as coalified compressions were observed (Fig. 4B).

The $\%C_{org}$ obtained after isotopic analyses is between 0.15 and 0.82 (Fig. 4), systematically showing slightly higher values than those obtained using Rock-Eval pyrolysis, but with the same trends. Higher values are recorded at the base of the core in lithological unit 1 which is enriched in continental organic matter. By comparison with unit 3, a slight increase is recorded in the interval corresponding approximately to lithological unit 2 (Fig. 5); however, significant enrichment in marine organic matter, which would have indicated it was preserved in a significantly oxygen-depleted environment, is not recorded.

The $\delta^{13}C_{org}$ values fluctuate between -24.19‰ and -27.91‰ (Fig. 4). A prominent negative excursion is recorded between 112 and 110 m at the base of lithological unit 2, followed by a shift to higher (close to -25‰) and relatively constant values up-section.

III-2. Clay mineralogy

The following main clay minerals were identified: a R0 type illite-smectite mixed-layer (17 Å based on a glycolated run condition) referred to as smectite for the following sections; chlorite (14.2 Å, 7.1 Å, 4.7 Å and 3.54 Å peaks); illite (10 Å, 5 Å, 3.33 Å peaks); kaolinite (7.18 Å and 3.58 Å peaks) and vermiculite (14 Å in air-drying conditions, 14.5-15 Å after ethylene-glycol solvation and 10 Å peaks after heating). In addition, traces of pyrophyllite are occasionally suspected by the occurrence of a small peak at 9.3 Å. The clay mineral assemblages are predominantly composed of illite generally between 40 and 50% and kaolinite with proportions comprised between 20 and 45%. Minor amounts of chlorite (less than 10%), vermiculite (around 10%) and smectite (generally less than 10%, except at the top of the formation where the proportions of this mineral may reach 50%) are associated with these two clay species (Fig. 6). Traces of pyrophyllite are only identified at the base of the

core. Four stratigraphic intervals can be distinguished according to the clay mineralogy. Interval 1 corresponds to the lowermost part of the formation below the bioclastic accumulation and coincides with lithological unit 1. In this interval, the proportion of vermiculite is relatively high and decreases up-section while the proportion of illite increases. The second interval, from 112 to 104.5 m is characterised by the relative abundance of kaolinite (30 to 45%) notably at the base of this interval where the proportions of this mineral show a maximum (45%), and by the absence of smectite. The third interval from 104.5 m to 87.5 m shows a monotonous clay assemblage without any significant change and is composed of approximately 5% of chlorite, 45% of illite, 10% of vermiculite, 10% of smectite and 30% of kaolinite. The uppermost part of the formation (interval 4) shows a sharp increase in the proportions of smectite balanced by significant decreasing proportions of illite and kaolinite.

IV - Discussion

IV-1. Depositional environments of the Argiles à Plicatules Formation

The lowermost part of the formation overlying the continental Wealden facies and consisting of dark grey clays with abundant iron oolites (Fig. 4A) and common terrestrial plant remains (woods and foliar remains, Fig. 4B) likely corresponds to transgressive sediments deposited in coastal environments. Similar facies were described in boreholes drilled close to Soulaines to the east of Juzanvigny (Fig. 2) where transgressive facies are clearly separated by emersion features suggesting, several transgressive events at the beginning of the Aptian transgression (Ferry, 2000). Foliar meso- and macro-remains exclusively consist of fragments of pinnae and isolated fern pinnules preserved as coalified compressions (Fig. 4B). The largest pinna fragment is 22 mm long. The pinnae bear up to 8 mm long and 3 mm wide alternate to subopposite, oblong, thick and leathery pinnules. They are attached by a broad base to the rachis and display a rounded apex and an entire margin.

Sometimes the pinnules are slightly inclined forward. The midrib is straight and ends before the apex of the pinnule. These features as well as the reticulate veins allow to ascribe these specimens to *Weichselia reticulata* (Stokes and Webb) Fontaine which is a common fern in the Early Cretaceous flora from Europe (Blanco-Moreno et al., 2018). In France, *W. reticulata* was previously reported from the Wealden facies of the Nord department (Carpentier, 1927) and the Oise department (Carpentier, 1929). The abundance of plant remains in oolithic facies shows that the depositional environment was influenced by strong terrestrial inputs. Although *Weichselia* mostly occurred in a continental environment in Europe (Blanco-Moreno et al., 2018), this report shows that *W. reticulata* was one of the components of littoral flora during the earliest Aptian.

As they occur immediately above the upper Barremian lateritic palaeo-alteration, iron oolites may be reworked from the lateritic soils (Bhattacharyya, 1983). However, iron oolites may also have formed as a replacement of a pre-existing ooid structure or via the precipitation of an iron aluminosilicate (chamosite/berthierine) grain in shallow marine environments (Velde, 1989). Iron may be provided in the sedimentary environment by the weathering of the proximal continental areas. In most cases iron oolites are associated with transgressive deposits, which is the case in the lowermost part of the Argiles à Plicatules Formation, and are indicators of condensed sections (Collin et al., 2005; Clement et al., 2020).

Up-section, the deposits increasingly less silty show common bivalves. The first ammonite occurs at 113.70 m indicating open-marine environments. The prominent shell horizon intercalated in the clayey succession at the top of lithological unit 1 between 112.40 m and 111.90 m (Fig. 4C) can be divided into two parts. The first corresponds to a bed comprising pluri-centimetric bivalve shells forming the base of a 30 cm-thick fining up sequence. The top of this bed, which is 112.05 m (Fig. 4C), is bioturbated. Above, a second accumulation of bivalves is associated with centimetric clasts. The succession may

301 correspond to two successive storm deposits separated by a bioturbated surface. This suggests
302 a deposition above storm wave base in upper offshore environments and a deepening trend of
303 the basin as a consequence of the Aptian transgression. This trend continues up-section from
304 111.90 m to 106.30 m, as the homogenous faintly bioturbated clays without any sedimentary
305 structure suggest a deposition in a quiet environment, below the storm wave base (lower
306 offshore). Rare calcareous nannofossils observed in smear slides occur in most of the samples
307 and are likely responsible for the carbonate content (close to 3%) of the sediment. From
308 106.30 m to the top of the formation, the clays contain more silt. Bioturbated surfaces indicate
309 sedimentation breaks that are consistent with the common occurrence of phosphate
310 (carbonate-apatite) nodules.

311 The Argiles à Plicatules Formation encompasses a transgressive interval from the base
312 to a maximum flooding surface located in the interval between 111.90 m and 106.30 m. The
313 uppermost 20 m of the formation corresponds to a highstand system tract terminated by a
314 prominent bioturbated surface between the Argiles à Plicatules and the Sables Verts de l'Aube
315 formations deposited at a shallower water depth in shoreface environments.

316

317 IV-2. Evolution of the $\delta^{13}C_{org}$ and organic matter contents

318 Several of the isotopic segments initially distinguished by Menegatti et al. (1998)
319 across the "Livello Selli", which includes OAE1a, or its equivalent in the Tethys Ocean, and
320 which were subsequently recognised worldwide and used as a reliable tool for
321 chemostratigraphic correlations, are clearly identified in the studied borehole: C2 at the base
322 of the section, C3 corresponding to the negative excursion showing the lowest values of
323 $\delta^{13}C_{org}$ between 111.80 and 110 m, C4, C5 and C6 characterised by a shift to higher values
324 and finally C7 (Fig. 5).

325 The 3‰ negative excursion that occurs immediately before OAE1a and corresponding
326 to the C3 segment is clearly identified. It occurs probably in the *deshayesi* Zone just above the
327 bioclastic accumulations interpreted as storm deposits, with an amplitude comparable to that
328 observed in many sedimentary basins (Menegatti et al., 1998; Ando et al., 2008). The C3
329 segment is relatively thick (1.80 m) indicating a relatively high sedimentation rate and shows
330 two distinct negative excursions separated by a positive excursion with a small amplitude,
331 which can also be observed in the $\delta^{13}C_{carb}$ curves from sections from south-east France (Kuhnt
332 et al., 1998; 2011). This may suggest the existence of, at least, two successive volcanic CO_2
333 pulses at the origin of the emplacement of the Ontong Java-Manihiki-Hikurangi Plateau
334 (Lorenzen et al., 2013; Naafs et al., 2016).

335 Surprisingly, the interval corresponding to the $\delta^{13}C_{org}$ positive excursion is not
336 significantly enriched in organic matter and the facies of the Argiles à Plicatules Formation
337 are extremely homogeneous, unchanged in colour and without any laminations. The absence
338 of significant organic matter enrichment is surprising since the deep, quiet lower offshore
339 depositional environment was favourable to the preservation of marine organic matter. Some
340 authors report an absence of significant marine organic matter enrichment in several
341 sedimentary basins of northern Spain including the Basco-Cantabric Basin (Garcia-Mondejar
342 et al., 2015) and the Organyà Basin (Sanchez-Hernandez and Maurasse, 2016) although they
343 correspond to oxygen-depleted environments but without prolonged anoxia.

344 In the Paris Basin, the absence of OM enrichment can be explained in several ways.

345 1) The primary productivity was probably low as suggested by the very low carbonate
346 content of the succession. The carbonate fraction of the Argiles à Plicatules Formation, which
347 does not exceed 4%, is composed of rare nannofossils including the genus *Watznaueria*,
348 *Zeugrhabdotus*, *Rhagodiscus*, *Biscutum, Discorhabdus* and *Cyclagelosphaera* (F. Giraud, *in*

Ferry, 2000). The scarcity of fauna and flora suggests that the environment must have been oligotrophic.

2) The absence of anoxia in the Aptian sea-way between the LBM/RM and the AM/MC (Fig. 1) may be also explained by the presence of marine currents flowing through the strait thus favouring relatively well-oxygenated environments. However, except the occasional occurrence of phosphate nodules that may indicate low sedimentation rate due to the winnowing of fine particles, there is no evidence of hydrodynamic influences expressed in the sedimentary facies.

3) The oxygen-minimum zone that was clearly expressed in the Tethys Ocean was deeper and did not reach the relatively shallow environments of the Paris Basin. This is plausible, given that Coccioni et al. (1987) and Westermann et al. (2013) show that anoxic to euxinic conditions developed in the deeper part of the Tethys Ocean during OAE 1a, while conditions were not as reducing in shallower environments.

By comparison with several sections from the Tethys ocean, the $\delta^{13}C_{org}$ positive excursion is less pronounced than expected, what could be the result of several gaps coeval with the positive excursion like those observed in carbonate platform environments (Wissler et al., 2005). However, except the occurrence of bioturbated surfaces and some scattered phosphate nodules, there is no clear evidence of significant sedimentation breaks.

IV-3. Significance of clay mineral assemblages

IV-3-1. Diagenetic influences

Before examining the significance of clay mineral assemblages in terms of the palaeoclimate and palaeoenvironment, it is essential to ensure that they are predominantly detrital in origin without any significant influence of burial diagenesis, thermal influences or authigenic growth during early or late diagenesis. The post-Aptian sedimentary successions

probably never exceeded 1100 m (Robaszynski et al., 2005), which is consistent with a weak thermal impact (Torelli et al., 2020) compatible with the occurrence of smectite and immature organic matter. Consequently, it is unlikely that clay minerals may have been transformed during burial diagenesis. This conclusion is consistent with many studies performed to the east of the Paris Basin on upper Jurassic deposits showing that the thermal influences remain very weak even when these deposits are more deeply buried (Pellenard et al., 1999; Pellenard and Deconinck, 2006; Blaise et al., 2014; Mangenot et al., 2018).

Small quantities of glauconite commonly occur in the uppermost part of the Argiles à Plicatules Formation at the transition with the overlying Sables verts de l'Aube Formation. Glauconite is an iron-rich illite and the granules are coarser than the clay fraction and normally not included in the clay fraction. However, as the samples are ground in preparation for XRD analyses, it is possible that glauconite was partly introduced in the clay fraction and slightly increases the total proportion of illite at the top of the formation.

Therefore, we assume that most clay minerals are detrital in origin and may be useful to precise environmental conditions that prevailed during the early Aptian around the Paris Basin.

IV-3-2. Environmental control of the clay sedimentation

Primary minerals, including illite, chlorite and pyrophyllite constitute more than half of the clay fraction. The abundance of these minerals suggests a relatively intense erosion on the continental areas bordering the Paris Basin. Although clay minerals may be transported over long distances, they likely originated from the Palaeozoic massifs surrounding the Paris Basin. Illite, chlorite and pyrophyllite originated from the erosion of igneous and metamorphic rocks from the AM/MC and from the low grade metamorphic rocks from the

LBM. Vermiculite is also common, notably at the base of the formation. This mineral also occurs in lower to middle Albian clayey strata of the Paris Basin and likely originated from the north, i.e. from the LBM (Gale et al., 1996; Corentin et al., 2020). Vermiculitic clays corresponding to illite/vermiculite mixed-layers were also identified together with illite and kaolinite in the Aptian deposits of the Lower Saxony Basin of Germany (Benesch et al., 1998) and likely originate from the moderate weathering of chlorite.

Kaolinite is also abundant with maximum values in interval 2 characterised by the homogeneous clay deposited in the deepest environments. Therefore, in the present case, the abundance of kaolinite cannot be a consequence of its preferential deposition in nearshore environments as suggested by Godet et al., (2008). The stratigraphic interval coinciding with the $\delta^{13}C_{org}$ negative excursion is strongly depleted in smectite suggesting that a particularly hydrolysing (warm and humid) climate was established at that time (Chamley, 1989; Ruffell et al., 2002). By contrast, in the topmost part of the Argiles à Plicatules Formation, the decreasing proportions of kaolinite balanced by increasing proportions of smectites suggest increasingly arid climate conditions confirming a certain variability in the Aptian climate (Dumitrescu et al., 2006; Bottini et al., 2015; Naafs and Pancost, 2016). These arid climatic conditions also seem to have prevailed during the Aptian-Albian in the Algarve Basin (Southern Portugal) where sedimentary rocks are depleted in kaolinite and show a high amount of the xerophytic pollen *Classopollis* (Heimhofer et al., 2008). Aridity may be a consequence of colder climate (cold snaps) recorded at the Aptian/Albian transition (Mutterlose et al., 2009; Maurer et al., 2012; Millán et al., 2014).

IV.4. Climate evolution during the deposition of the Argiles à Plicatules Formation

A comparison of $\delta^{13}C_{org}$ and the mineralogical data shows that the C3 segment corresponding to the negative excursion recorded prior to the OAE1a is characterised by an

424 increase in the proportions of kaolinite (Fig. 7) at the same time as a decrease in the
425 proportions of smectites. This suggests the installation of a more humid climate as a
426 consequence of an acceleration of the hydrological cycle induced by the warming triggered by
427 the increase in pCO_2 (Keller et al., 2011; Bodin et al., 2015; Naafs and Pancost, 2016). There
428 are several lines of evidence for such a climatic change. Wortmann et al. (2004) suggested
429 that the widespread occurrence of sandstones in the Tethys-Atlantic seaway was a
430 consequence of increasing erosion rates due to the acceleration of the hydrological cycle in
431 the wake of the early Aptian carbon cycle perturbation. Increasing global weathering intensity
432 coeval with OAE1a is also suggested by calcium isotopes (Blättler et al., 2011) measured in
433 carbonate deposits from several areas including southern England, Italy and Resolution Guyot
434 from the mid-pacific mountains. Hochuli et al. (1999) also describe global warming resulting
435 in increasing riverine fluxes. The warming is evidenced by a drop in $\delta^{18}O$, TEX_{86} data and by
436 pollen records. The $\delta^{18}O$ data from many sedimentary basins including the South Pacific
437 shows, that the ocean waters warmed strongly during the negative excursion and that
438 temperatures then decreased probably due to the storage of organic matter in the sediments
439 (Ando et al., 2008; Stein et al., 2011; Zakharov et al., 2013). These observations are in
440 agreement with the maximum proportions of kaolinite and the decrease in the proportion of
441 *Classopollis*, (xerophytic pollen) in the Maestrat Basin (eastern Spain) during OAE1a (Cors et
442 al. 2015). Tex_{86} data obtained in the Selli level (or other equivalents of the OAE1a) also
443 indicate particularly warm sea-surface temperatures (Schouten et al., 2003; Dumitrescu and
444 Brassel, 2006; Mutterlose et al., 2010, 2014).

445 The global warming that occurred prior to OAE1a is therefore likely responsible for an
446 acceleration of the hydrological cycle and for the increase of kaolinite because of increasing
447 runoff and hydrolyses on the continental areas bordering the Paris Basin. The high
448 proportions of kaolinite in Aptian deposits of the Paris Basin could be explained by the

449 formation of kaolinite in soils, but the duration of the climatic perturbation is relatively short,
450 between 280 and 350 kyr (Lorenzen et al., 2013), while the formation of kaolinite in soils
451 required a longer time estimated at least to 1 myr (Thiry, 2000). It is more likely that kaolinite
452 was principally reworked from kaolinite-rich weathering profiles developed over the
453 Palaeozoic massifs during the Early Cretaceous (Jurassic-Cretaceous transition to Barremian)
454 (Meyer, 1976; Gilg, 2000; Quesnel, 2003; Yans, 2003; Thiry et al., 2005, 2006; Corentin et
455 al., 2020). As detrital clays including kaolinite may be reworked from older rocks or from
456 palaeo-alterations, their climatic significance may be questioned (Jeans et al., 2001), but
457 overall, illite and kaolinite dominated clay assemblages of the Aptian in the Paris Basin point
458 to a significant runoff and consequently to humid climate conditions. It is probable, that
459 fluctuations in the hydrological cycle controlling fluvial inputs occurred before and during
460 OAE1a as evidenced by changing environmental conditions in terms of anoxia/dysoxia
461 (Socorro and Maurasse, 2018; 2020).

462 Although the reliability of $\delta^{18}O$ data has recently been confirmed (O'Brien et al.,
463 2017), the acceleration of the hydrological cycle following the very hot episode preceding
464 OAE1a can be used to address the question of the significance of the low $\delta^{18}O$ values
465 recorded prior to OAE1a. $\delta^{18}O$-values may also be a result of a slight decrease in ocean
466 salinity. This question, already addressed for other periods, shows that it is essential to take
467 better account of the fluctuations in the hydrological cycle in the context of climatic
468 reconstructions. In addition, higher runoff may increase thermohaline stratification that may
469 be involved in the development of an OAE (e.g. Erbacher et al., 2001; Van Helmond et al.,
470 2015).

471

472 Conclusions

For the first time, OAE1a is clearly identified in argillaceous deposits, the so-called Argiles à Plicatules Formation, deposited in the Paris Basin. Most of the C-isotope segments defining the OAE 1a interval are identified in the stratigraphic succession. However, the section is devoid of any significant marine organic matter enrichment likely because the Tethyan oxygen-depleted deep-water masses did not reach the epicontinental areas of the Paris Basin. The global warming preceding OAE1a is likely responsible for an acceleration of the hydrological cycle, an increase in runoff and the reworking of kaolinite from palaeoweathering profiles cropping out on the Palaeozoic massifs bordering the Paris Basin. As indicators for an acceleration of the hydrological cycle are also recorded in other areas, a slight decrease in ocean salinity prior to OAE1a may be responsible in part for its development and questions the reliability of the sea surface temperature deduced from the $\delta^{18}O$ values. The hydrolysing conditions were so intense prior to and during OAE1a that smectite totally disappeared from the clay fraction. However, smectite increases in the upper part of the succession suggesting, that more arid conditions prevailed at that time possibly in relation with a colder climate during the Aptian/Albian transition. The changing clay mineral assemblages suggest, that the Aptian stage was characterised by a climate instability marked not only by changes in temperature but also in the hydrological cycle.

Acknowledgements: We would like to thank Claude Aurière, who is in charge of storing Andra's cores, for his help in studying the boreholes. We would like to warmly thank the two reviewers, Jochen Erbacher and Helmut Weissert for their constructive and helpful comments on the initial version of the manuscript.

References

Allen, P., 1998. Purbeck-Wealden (early Cretaceous) climates. Proceedings of the Geologists' Association 109, 197–236.

Amédro, F., Matrion, B., Deconinck, J.F., Huret, E. Landrein, P., 2017. Les forages de Juzanvigny (Aube, France) : litho-biostratigraphie des formations du Barrémien à l'Albien moyen dans l'est du bassin de Paris et datations par les ammonites. Geodiversitas 39, 2, 185-212.

Amodio, S., Weissert, H., 2017. Palaeoenvironment and palaeoecology before and at the onset of Oceanic Anoxic Event (OAE)1a: Reconstructions from Central Tethyan archives. Palaeogeography, Palaeoclimatology, Palaeoecology 479, 71–89.

Ando, A., Kaiho, K., Kawahata, H., Kakegawa, T., 2008. Timing and magnitude of early Aptian extreme warming: Unraveling primary $\delta^{18}O$ variation in indurated pelagic carbonates at Deep Sea Drilling Project Site 463, central Pacific Ocean. Palaeogeography, Palaeoclimatology, Palaeoecology 260, 463–476.

Baudin, F., 1996. Enregistrement de l'événement anoxique aptien inférieur dans les faciès péritidaux du Guyot Resolution (océan Pacifique Nord-Ouest). C.R Acad. Sci., Paris 323 (IIa), 221-228.

Behar, F., Beaumont, V., De B. Penteado, H.L., 2001. Technologie Rock-Eval 6 : performances et développements. Oil and Gas Science and Technology, Revue de l'Institut Français du Pétrole 56, 111–134.

Bellanca, A., Erba, E., Neri, R., Premoli Silva, I., Sprovieri, M., Tremolada, F., Verga, D., 2002. Palaeoceanographic significance of the Tethyan "Livello Selli" (early Aptian) from the Hybla Formation, northwestern Sicily: biostratigraphy and high-resolution chemostratigraphic records. Palaeogeography, Palaeoclimatology, Palaeoecology 185, 175–196.

522 Benesch, M., Heydemann, A., Usdowski, E., 1998. Mineralogy of the Lower Aptian
523 sediments from the borehole Hoheneggelsen KB 40, with special emphasis on the clay
524 mineralogy. Cretaceous Research 19, 569-580.
525 Blaise, T., Barbarand, J., Kars, M., Ploquin, F., Aubourg, C., Brigaud, B., Cathelineau, M., El
526 Albani, A., Gautheron, C., Izart, A., Janots, D., Michels, R., Pagel, M., Pozzi, J.P.,
527 Boiron, M.C., Landrein, P., 2014. Reconstruction of low temperature (<100° C) burial
528 in sedimentary basins: A comparison of geothermometer in the intracontinental Paris
529 Basin. Marine and Petroleum Geology 53, 71-87.
530 Blanco-Moreno, C., Gomez, B., Buscalioni, Á., 2018. Palaeobiogeographic and metric
531 analysis of the Mesozoic fern *Weichselia*. Geobios 51(6), 571-578.
532 Blättler, C.L., Jenkyns, H.C., Reynard, L.M., Henderson, G.M., 2011. Significant increases in
533 global weathering during Oceanic Anoxic Events 1a and 2 indicated by calcium
534 isotopes. Earth and Planetary Science Letters 309, 77–88
535 Bodin, S., Meissner, P., Janssen, N.M.M., Steuber, T., Mutterlose, J., 2015. Large igneous
536 provinces and organic carbon burial: Controls on global temperature and continental
537 weathering during the Early Cretaceous. Global and Planetary Change 133, 238–253.
538 Bottini, C., Cohen, A.S., Erba, E., Jenkyns, H.C., Coe, A.L., 2012. Osmium-isotope evidence
539 for volcanism, weathering, and ocean mixing during the early Aptian OAE 1a.
540 Geology 40, 583–586.
541 Bottini, C., Erba, E., Tiraboschi, D., Jenkyns, H.C., Schouten, S., Sinninghe Damsté, J.S.,
542 2015. Climate variability and ocean fertility during the Aptian Stage. Climate of the
543 Past 11, 383-402.
544 Bréhéret, J.G., 1997. L'Aptien et l'Albien de la Fosse vocontienne (des bordures au bassin).
545 Évolution de la sédimentation et enseignements sur les événements anoxiques. Société
546 Géologique du Nord, Publ. n° 25, 644 p.

547 Carpentier, A., 1927. La flore wealdienne de Féron-Glageon (Nord). Mémoires de la Société
548 Géologique du Nord 1, 1–151.
549 Carpentier, A., 1929. Recherches sur les végétaux fossiles des argiles éocrétaciques du Pays
550 de Bray. Bulletin de la Société Géologique de France 4(29), 89-96.
551 Casey, R., 1961. The stratigraphical paleontology of the Lower Greensand. Palaeontology,
552 London 3, 487-621, pl. 77-84.
553 Chamley, H., 1989. Clay sedimentology. Springer, Berlin, Heidelberg, 623 p.
554 Charbonnier, G., Föllmi, K.G., 2017. Mercury enrichments in lower Aptian sediments support
555 the link between Ontong Java large igneous province activity and oceanic anoxic
556 episode 1a. Geology 45, 1, 63-66.
557 Clement, A.M., Tackett, L.S., Ritterbush, K.A., Ibarra, Y., 2020. Formation and stratigraphic
558 facies distribution of early Jurassic iron oolite deposits from west central Nevada,
559 USA. Sedimentary Geology 395, 105537.
560 Coccioni, R., Erba, E., Premoli Silva, I., 1992. Barremian-Aptian calcareous plankton
561 biostratigraphy from the Gorgo a Cerbara section (Marche, Central Italy) and
562 implication for planktonic evolution. Cretaceous Research 13, 517-537.
563 Coccioni, R., Nesci, O., Tramontana, M., Wezel, F.C., Moretti, E., 1987. Descrizione di un
564 livello guida “radiolaritico-bituminoso-ittiolitico” alla base delle Marne a Fucoidi
565 nell’Appennino Umbrio-Marchigiano. Bollettino della Società geologica italiana 106,
566 1, 183-192.
567 Collin, P., Loreau, J., Courville, P., 2005. Depositional environments and iron ooid formation
568 in condensed sections (Callovian–Oxfordian, south-eastern Paris basin, France).
569 Sedimentology 52, 969–985.

570 Cors, J., Heimhofer, U., Adatte, T., Hochuli, P.A., Huck, S., Bover-Arnal, T., 2015. Climatic
571 evolution across oceanic anoxic event 1a derived from terrestrial palynology and clay
572 minerals (Maestrat Basin, Spain). Geological Magazine 152, (4), 632–647.
573 Corentin, P., Deconinck, J.F., Pellenard, P., Amédro, F., Bruneau, L., Chenot, E., Matrion, B.,
574 Huret, E., Landrein, P., 2020. Environmental and climatic controls of the clay
575 mineralogy of Albian deposits in the Paris and Vocontian basins (France). Cretaceous
576 Research 108, https://doi.org/10.1016/j.cretres.2019.10434.
577 Dumitrescu, M., Brassell, S.C., 2006. Compositional and isotopic characteristics of organic
578 matter for the Early Aptian Oceanic Anoxic Event at Shatsky Rise, ODP Leg 198.
579 Palaeogeography, Palaeoclimatology, Palaeoecology 235, 168–191.
580 Dumitrescu, M., Brassell, S.C., Schouten, S., Hopmans, E.C., Sinninghe Damsté, J.S., 2006.
581 Instability in tropical Pacific sea-surface temperatures during the early Aptian.
582 Geology 34, 10, 833–836.
583 Erba, E., 1994. Nannofossils and superplumes: the early Aptian "nannoconid crisis.
584 Paleoceanography 9, 483–501.
585 Erba, E., 2004. Calcareous nannofossils and Mesozoic oceanic anoxic events. Marine.
586 Micropaleontology 52, 85–106.
587 Erba, E., Duncan, R.A., Bottini, C., Tiraboschi, D., Weissert, H., Jenkyns, H.C., Malinverno,
588 A., 2015. Environmental consequences of Ontong Java Plateau and Kerguelen Plateau
589 volcanism. In Geological Society of America Special Papers, Vol. 511. Geological
590 Society of America, 271–303 pp.
591 Erbacher, J., Thurow, J., Littke, R., 1996. Evolution patterns of radiolarian and organic matter
592 variations: a new approach to identify sea-level changes in mid-Cretaceous pelagic
593 environments. Geology 24, 499–502.

Erbacher, J., Huber, B. T., Norris, R. D., Markey, M., 2001. Increased thermohaline stratification as a possible cause for an ocean anoxic event in the Cretaceous period. Nature 409, 325–327.

Espitalié, J., 1986. Use of Tmax as a maturation index for different types of organic matter. Comparison with vitrinite reflectance. In: Thermal Modelling in Sedimentary Basins. Technip, Paris, pp. 475–496.

Espitalié, J., La Porte, J.L., Madec, M., Marquis, F., Le Plat, P., Paulet, J., Boutefeu, A., 1977. Rapid method for source rocks characterization and for determination of petroleum potential and degree of evolution. Oil and Gas Science and Technology, Revue de l'Institut Français du Pétrole 32, 23–42.

Ferry, S., 2000. Analyse sédimentologique de la série albo-aptienne de Soulaines – Projet site TFA. Unpublished report n° F RP O UCB TFA 00-204/A, Andra, 62 p.

Föllmi, K.B., 2012. Early Cretaceous life, climate and anoxia. Cretaceous Research 35, 230-257.

Gale, A.S., Huggett, J.M., Gill, M., 1996. The stratigraphy and petrography of the Gault Clay Formation (Albian, Cretaceous) at Redcliff, Isle of Wight. Proceedings of the Geologists' Association 107, 287-298.

Garcia-Mondejar, J., Fernandez-Mendiola, P.A., Owen, H.G., 2015. The OAE1a in Cuchia (Early Aptian, Spain): C and O geochemistry and global correlation. Acta Geologica Polonica 65, (4), 525–543.

Gilg, A. 2000. D–H evidence for the timing of kaolinization in Northeast Bavaria, Germany. Chemical geology 170, 5 – 18.

Giraud, F., Pittet, B., Grosheny, D., Baudin, F., Lécuyer, C., Sakamoto, T., 2018. The palaeoceanographic crisis of the Early Aptian (OAE 1a) in the Vocontian Basin (SE France). Palaeogeography, Palaeoclimatology, Palaeoecology 511, 483–505.

619 Godet, A., Bodin, S., Adatte, T., Föllmi, K.B., 2008. Platform-induced clay-mineral
620 fractionation along a northern Tethyan basin-platform transect: implications for the
621 interpretation of Early Cretaceous climate change (Late Hauterivian-Early Aptian).
622 Cretaceous Research 29, 830–847.
623 Godet, A., Hfaiedh, A., Arnaud-Vanneau, A., Zghal, I., Arnaud, H., Ouali, J., 2014. Aptian
624 palaeoclimates and identification of an OAE1a equivalent in shallow marine
625 environments of the southern Tethyan margin: Evidence from Southern Tunisia (Bir
626 Oum Ali section, Northern Chott Chain). Cretaceous Research 48, 110-129.
627 Graziano, R., 2013. Sedimentology, biostratigraphy and event stratigraphy of the Early Aptian
628 Oceanic Anoxic Event (OAE1A) in the Apulia Carbonate Platform Margin - Ionian
629 Basin System (Gargano Promontory, southern Italy). Cretaceous Research 39, 78-111.
630 Guillocheau, F., Robin, C., Allemand, P., Bourquin, S., Brault, N., Dromart, G., Friedenberg,
631 R., Garcia, J.-P., Gaulier, J.-M., Gaumet, F., Grosdoy, B., Hanot, F., Le Strat, P..,
632 Mettraux, M., Nalpas, T., Prijac, C., Rigollet, C., Serrano, O., Granjean, G., 2000.
633 Meso-Cenozoic geodynamic evolution of the Paris Basin: 3D stratigraphic constraints.
634 Geodinamica Acta, 13, 189–245.
635 Heimhofer, U., Adatte, T., Hochuli, P.A., Burla, S., Weissert, H., 2008. Coastal sediments
636 from the Algarve: low-latitude climate archive for the Aptian-Albian. International
637 Journal of Earth Sciences (Geologishe Rundschau) 97, 785–797.
638 Hochuli, P.A., Menegatti, A.P., Weissert, H., Riva, A., Erba, E., Premoli Silva I., 1999.
639 Episodes of high productivity and cooling in the early Aptian Alpine Tethys. Geology
640 27/7, 657–660.
641 Hueter, A., Huck, S., Bodin, S., Heimhofer, U., Weyer, S., Jochum, K. P., Immenhauser, A.,
642 2019. Central Tethyan platform-top hypoxia during Oceanic Anoxic Event 1a. Climate
643 of the Past 15, 1327–1344.

644 Jacquin, T., Rusciadelli, G., Amédro, F., Graciansky, P.-C. de, Magniez-Jannin, F., 1998. The
645 north-Atlantic cycle: an overview of second order transgressive-regressive facies
646 cycles in Western Europe. *In* P.-C. de Graciansky, J. Hardenbol, T. Jacquin and P.R.
647 Vail (Eds), Cenozoic and Mesozoic Sequence Stratigraphy of European Basins.
648 *S.E.P.M., Special Publication,* 60, 397-409.
649 Jenkyns, H.C., 2010. Geochemistry of oceanic anoxic events. Geochemistry, Geophysics,
650 Geosystems, 11, 3.
651 Keller, C.E., Hochuli, P.A., Weissert, H, Bernasconi, S.M., Giorgioni, M., Garcia, T.I., 2011.
652 A volcanically induced climate warming and floral change preceded the onset of
653 OAE1a (Early Cretaceous). Palaeogeography, Palaeoclimatology, Palaeoecology 305,
654 43–49.
655 Kuhnt, W., Holbourn, A., Moullade, M., 2011. Transient global cooling at the onset of early
656 Aptian oceanic anoxic event (OAE) 1a. Geology 39, 4, 323–326.
657 Kuhnt, W., Moullade, M., Masse, J.P., Erlenkeuser, H., 1998. Carbon isotope stratigraphy of
658 the lower Aptian historical stratotype at Cassis– La Bédoule (SE France): Géologie
659 Méditerranéenne, 25, 63–79.
660 Lafargue, E., Marquis, F., Pillot, D., 1998. Les applications de Rock-Eval 6 dans l'exploration
661 et la production des hydrocarbures, et dans les études de contamination des sols. Oil
662 and Gas Science and Technology, Revue de l'Institut Français du Pétrole 53, 421–
663 437.
664 Larson, R.L., Erba, E., 1999. Onset of the mid-Cretaceous greenhouse in the Barremian-
665 Aptian: igneous events and the biological, sedimentary and geochemical responses.
666 Paleoceanography 14, 663–678.

667 Leckie, R. M., Bralower, T. J., Cashman, R., 2002. Oceanic anoxic events and plankton
668 evolution: Biotic response to tectonic forcing during the mid-Cretaceous:
669 Paleoceanography, 17, 13-1-13–29.
670 Li, Y.X., Bralower, T.J., Montañez, I.P., Osleger, D.A., Arthur, M.A., Bice, D.M., Herbert,
671 T.D., Erba, E., Premoli Silva, I., 2008. Toward an orbital chronology for the early
672 Aptian Oceanic Anoxic Event (OAE1a, ~120 Ma). Earth and Planetary Science Letters
673 271, 88–100.
674 Lorenzen, J., Kuhnt, W., Holbourn, A., Flögel, S., Moullade, M., Tronchetti, G., 2013. A new
675 sediment core from the Bedoulian (Lower Aptian) stratotype at Roquefort-La Bédoule,
676 SE France. Cretaceous Research 39, 6–16.
677 Luciani, V., Cobianchi, M., Lupi, C., 2006. Regional record of a global oceanic anoxic event:
678 OAE1a on the Apulia Platform margin, Gargano Promontory, southern Italy.
679 Cretaceous Research 27, 754-772.
680 Mangenot, X., Gasparrini, M., Gerdes, A., Bonifacie, M., Rouchon, V., 2018. An emerging
681 thermochronometer for carbonate-bearing rocks: Δ47 /(U-Pb). Geology 46, 1067–
682 1070.
683 Masse, J. P., Bouaziz, S., Amon, E. O., Baraboshkin, E., Tarkowski, R., Bergerat, F.,
684 Sandulescu, M., Platel, J.P., Canérot, J., Guiraud, R., Poisson, A., Ziegler, M.,
685 Rimmele, G., Map 13. Early Aptian. (112-114 Ma) *Peri-Tethys programme,*
686 *paleogeographical atlas. Commission de la Carte Géologique du Monde/Commission*
687 *for the Geologic Map of the World, Paris*, 2000.
688 Maurer, F., van Buchem, F.S.P., Eberli, G.P., Pierson, B.J., Raven, M.J., Larsen, P.H., Al-
689 Husseini, M. I., Vincent, B., 2012. Late Aptian long-lived glacio-eustatic lowstand
690 recorded on the Arabian Plate. Terra Nova 25, 87-94.
691 Méhay, S., Keller, C. E., Bernasconi, S. M., Weissert, H., Erba, E., Bottini, C., Hochuli, P. A.,

692 2009. A volcanic CO_2 pulse triggered the Cretaceous Oceanic Anoxic Event 1a and a
693 biocalcification crisis. Geology 37, 819–822.
694 Menegatti, A.P., Weissert, H., Brown, R.S., Tyson, R.V., Farrimond, P., Strasser, A., Caron,
695 M., 1998. High-resolution $\delta^{13}C$ stratigraphy through the early Aptian "Livello Selli" in
696 the Alpine Tethys. Paleoceanography 13, (5), 530-545.
697 Meyer, R., 1976. Continental sedimentation, soil genesis and marine transgression in the basal
698 beds of the Cretaceous in the east of the Paris Basin. Sedimentology 23, 235-253.
699 Millán, M.I., Weissert, H.J., López-Horgue, M.A., 2014. Expression of the late Aptian cold
700 snaps and the OAE1b in a highly subsiding carbonate platform (Aralar, northern
701 Spain). Palaeogeography, Palaeoclimatology, Palaeoecology 411, 167–179
702 Moore, D.M., Reynolds, R.C., 1997. X-Ray Diffraction and the Identification and Analysis of
703 Clay Minerals. Oxford University Press, New York, 378 p.
704 Mutterlose, J., Bornemann, A, Herrle, J.O., 2009. The Aptian – Albian cold snap: Evidence
705 for "mid" Cretaceous icehouse interludes Neues Jahrbuch für Geologie und
706 Paläontologie - Abhandlungen, 252, 217-225.
707 Mutterlose, J., Bottini, C., Schouten, S., Sinninghe Damsté, J. S., 2014. High sea-surface
708 temperatures during the early Aptian Oceanic Anoxic Event 1a in the boreal realm.
709 Geology 42, 439-442.
710 Mutterlose, J., Malkoc, M., Schouten, S., Sinninghe Damsté, J. S., Forster, A., 2010. TEX86
711 and stable $\delta^{18}O$ paleothermometry of Early Cretaceous sediments: implications for
712 belemnite ecology and paleotemperature proxy application. Earth and Planetary
713 Science Letters 298, 286–298.
714 Naafs, B. D. A., Castro, J. M., De Gea, G. A., Quijano, M. L., Schmidt, D. N., Pancost, R. D.,
715 2016. Gradual and sustained carbon dioxide release during Aptian Oceanic Anoxic
716 Event 1a. Nature Geoscience 9, 135–139.

717 Naafs, B.D.A., Pancost, R.D., 2016. Sea-surface temperature evolution across Aptian Oceanic
718 Anoxic Event 1a. Geology 44, 959–962.
719 Najarro, M., Rosales, I., Martín-Chivelet, J., 2011. Major palaeoenvironmental perturbation in
720 an Early Aptian carbonate platform: Prelude of the Oceanic Anoxic Event 1a?
721 Sedimentary Geology 235 50–71
722 O'Brien, C.L., Robinson, S.A., Pancost, R.D et al., 2017. Cretaceous sea-surface temperature
723 evolution: Constraints from TEX86 and planktonic foraminiferal oxygen isotopes.
724 Earth-Science Reviews 172, 224-247.
725 Pellenard, P., Deconinck, J.F., Marchand, D., Thierry, J., Fortwengler, D., Vigneron, G.,
726 1999. Contrôle géodynamique de la sédimentation argileuse du Callovien-Oxfordien
727 moyen dans l'Est du Bassin de Paris : influence eustatique et volcanique Comptes
728 Rendus de l'Académie des Sciences, Paris 328, 807-813
729 Pellenard, P., Deconinck, J.F., 2006. Mineralogical variability of Callovo-Oxfordian clays
730 from the Paris Basin and the Subalpine Basin. Compte Rendus Geoscience 338, 854-
731 866.
732 Pictet, A., Delanoy, G., Adatte, T., Spangenberg, J.E., Baudouin, C., Boselli, P., Boselli,
733 Kindler, P., Föllmi, K.G., 2015. Three successive phases of platform demise during
734 the early Aptian and their association with the oceanic anoxic Selli episode (Ardèche,
735 France). Palaeogeography, Palaeoclimatology, Palaeoecology 418, 101-125.
736 Quesnel, F., 2003. Paleoweathering and paleosurfaces from northern and eastern France to
737 Belgium and Luxembourg: geometry, dating and geodynamic implications. Géologie
738 de la France 1, 95-104.
739 Radley, J.D., Allen, P., 2012. The Wealden (non-marine Lower Cretaceous) of the Weald
740 Sub-basin, southern England. Proceedings of the Geologists' Association 123, 245-
741 318.

742 Reboulet, S. compiler 2018. Report on the 6th International Meeting of the IUGS Lower
743 Cretaceous Ammonite Working Group, the « Kilian Group » (Vienna, Austria, 20 th
744 August 2017). Cretaceous Research 91, 100-110.
745 Robaszynski, F., Pomerol, B., Masure, E., Bellier, J.P., Deconinck, J.F., 2005. Stratigraphy
746 and stage boundaries in a type-section of the Late Cretaceous chalk from the East Paris
747 basin: The "Craie 700 boreholes". Cretaceous Research 26, 2, 157-169.
748 Ruffell, A., McKinley, J.M., Worden, R.H., 2002. Comparison of clay mineral stratigraphy to
749 other proxy palaeoclimate indicators in the Mesozoic of NW Europe. Philosophical
750 Transactions of the Royal Society London A 360, 675-693.
751 Sanchez-Hernandez, Y., Maurasse, F.J.-M.R., 2016. The influence of regional factors in the
752 expression of oceanic anoxic event 1a (OAE1a) in the semi-restricted Organyà Basin,
753 south-central Pyrenees, Spain. Palaeogeography, Palaeoclimatology, Palaeoecology
754 441, 582–598.
755 Schlanger, S.O., Jenkyns, H.C., 1976. Cretaceous oceanic anoxic events: causes and
756 consequences. Geologie en Minjbouw 55, (3-4), 179-184.
757 Schouten, S., Hopmans, E.C., Forster, A., van Breugel, Y., Kuypers, M.M.M., Sinninghe
758 Damsté J.S., 2003. Extremely high sea-surface temperatures at low latitudes during the
759 middle Cretaceous as revealed by archaeal membrane lipids. Geology 31, 12, 1069–
760 1072.
761 Socorro, J., Maurrasse, F.J.-M.R., 2019. Continuous accumulation of organic matter-rich
762 sediments associated with Oceanic Anoxic Event 1a in the El Pujal section, Organyà
763 Basin, Catalunyà Spain and its relation to episodic dysoxia. Cretaceous Research 95,
764 225-251.
765 Socorro, J., Maurrasse, F.J.-M.R., 2020. Regional palaeoenvironmental influence on organic
766 matter sequestration and characteristics of carbon isotope segment C5 in a hemipelagic

767 sequence, Organyà Basin, northeast Spain. Depositional record, DOI:
768 10.1002/dep2.111.
769 Squires, R.L., Saul, L.R., 1997. Review of the bivalve genus *Plicatula* from Cretaceous and
770 lower Cenozoic strata of California and Baja California. Journal of Paleontology 71,
771 (2), 287-298.
772 Stein, M., Föllmi, K. B., Westermann, S., Godet, A., Adatte, T., Matera, V., Berner, Z., 2011.
773 Progressive palaeoenvironmental change during the Late Barremian–Early Aptian as
774 prelude to Oceanic Anoxic Event 1a: evidence from the Gorgo a Cerbara section
775 (Umbria-Marche basin, central Italy). Palaeogeography, Palaeoclimatology,
776 Palaeoecology 302, 396–406.
777 Tarduno, J.A., Sliter, W. V., Kroenke, L., Leckie, M., Mayer, H., Mahoney, J. J., Musgrave,
778 R., Storey, M., Winterer, E. L., 1991. Rapid Formation of Ontong Java Plateau by
779 Aptian Mantle Plume Volcanism. Science 254, 399-403.
780 Tejada, M. L. G., Suzuki, K., Kuroda, J., Coccioni, R., Mahoney, J. J., Ohkouchi, N.,
781 Sakamoto, T., Tatsumi, Y., 2009. Ontong Java Plateau eruption as a trigger for the
782 early Aptian oceanic anoxic event. Geology 37, 855–858.
783 Thiry, M., 2000. Palaeoclimatic interpretation of clay minerals in marine deposits: an outlook
784 from the continental origin. Earth-Science Reviews 49, (1-4), 201-221.
785 Thiry, M., Quesnel, F., Yans, J., Wyns, R., Vergari, A., Théveniaut, H., Simon-Coinçon, R.,
786 Ricordel, C., Moreau, M.G., Giot, D., Dupuis, C., Bruxelles, L., Barbarand, J., Baele,
787 J.M., 2006. Continental France and Belgium during the early Cretaceous:
788 paleoweatherings and paleolandforms. Bulletin de la Société Géologique de France
789 177, (3), 155-175.

790 Thiry, M., Simon-Coinçon, R., Quesnel, F. Wyns, R., 2005. Altération bauxitique associée
791 aux argiles à chailles sur la bordure sud-est du bassin de Paris. Bulletin de la Société
792 Géologique de France 176, (2), 199-214.
793 Torelli, M., Traby, R., Teles, V., Ducros, M., 2020. Thermal evolution of the intracratonic
794 Paris Basin: Insights from 3D basin modelling. Marine and Petroleum Geology 119,
795 104487.
796 Van Helmond, N.A.G.M., Sluijs, A., Sinninghe Damsté, J.S., Reichart, G.J., Voigt, S.,
797 Erbacher, J., Pross, J., Brinkhuis, H. 2015. Freshwater discharge controlled deposition
798 of Cenomanian–Turonian black shales on the NW European epicontinental shelf
799 (Wunstorf, northern Germany). Climate of the Past 11, 495–508.
800 Velde, B. 1989. Phyllosilicate formation in berthierine peloids and iron oolites. Geological
801 Society, London, Special Publications, 46, 3-8.
802 Vincent, B., van Buchem, F.S.P., Bulot, L.G., Immenhauser, A., Caron, M., Baghbani, D.,
803 Huc, A.Y., 2010. Carbon-isotope stratigraphy, biostratigraphy and organic matter
804 distribution in the Aptian – Lower Albian successions of southwest Iran (Dariyan and
805 Kazhdumi formations) GeoArabia Special Publication 4, 1, 139-197.
806 Westermann, S., Stein, M., Matera, V., Fiet, N., Fleitmann, D., Adatte, T., Föllmi, K.B., 2013.
807 Rapid changes in the redox conditions of the western Tethys Ocean during the early
808 Aptian oceanic anoxic event. Geochimica et Cosmochimica Acta 121, 467–486.
809 Wissler, L., Funk, H., Weissert, H., 2003. Response of Early Cretaceous carbonate platforms
810 to changes in atmospheric carbon dioxide levels. Palaeogeography, Palaeoclimatology,
811 Palaeoecology 200, 187-205.
812 Wortmann, U.G., Herrle, J.O., Weissert, H. 2004. Altered carbon cycling and coupled
813 changes in Early Cretaceous weathering patterns: Evidence from integrated carbon

isotope and sandstone records of the western Tethys. Earth and Planetary Science Letters 220, 69-82.

Yans, J. 2003. An overview of the saprolites of Belgium and their potential kaolinitic supplies to Mesozoic and Cainozoic sediments. Géologie de la France 1, 33-37.

Zakharov, Y.D., Baraboshkin, E.Y., Weissert, H., Michailova, I. A., Smyshlyaeva, O.P., Safronova, P. P., 2013. Late Barremian-early Aptian climate of the northern middle latitudes: Stable isotope evidence from bivalve and cephalopod molluscs of the Russian Platform. Cretaceous Research 44, 183-201.

Figure captions

Fig. 1. Palaeogeographic map modified from R. Blakey: https://www2.nau.edu/rcb7/.
AM = Armorican Massif, MC = Massif Central, LBM = London Brabant Massif, RM = Rhenish Massif, BM = Bohemian Massif, CSM = Corso-Sardinia Massif, AB = Algarve Basin, PB = Paris Basin, LSB = Lower Saxony Basin.

Fig. 2. Simplified geological map of the area to the east of the Paris Basin and location of the AUB 121 borehole near Juzanvigny.

Fig. 3. Lithology of the AUB 121 borehole from the lower Barremian “Argiles ostréennes” Formation to the lowermost part of the “Argiles tégulines de Courcelles” Formation (lower Albian) (modified after Amédro et al., 2017). The lower Aptian Argiles à Plicatules Formation comprises three distinct lithological units and are dated by ammonites. The *deshayesi* and *furcata* ammonite Zones are clearly identified while the

838 lowermost part of the formation may belong to the *forbesi* Zone (see text). (A.P. =
839 Argiles à Plicatules).
840
841 Fig. 4. Base of the "Argiles à Plicatules" Formation. A. Thin section showing an iron oolite in
842 a clayey matrix with quartz grains (Q) (sample AUB 121 116.70 m). B. sample AUB
843 121, at an altitude of 116.60 m, shows abundant plant debris and notably *Weichselia*
844 *reticulata*. C. Picture of the core showing the top of Unit 1 (grey clays) with the
845 prominent shelly beds, and the base of Unit 2 (grey-brown clays).
846
847 Fig. 5. $CaCO_3$ content, $\%C_{org}$ and $\delta^{13}C_{org}$ stratigraphic trends along the "Argiles à Plicatules"
848 Formation. The prominent $\delta^{13}C_{org}$ negative excursion occurring prior to the OAE1a is
849 compared with the $\delta^{13}C_{org}$ of the Roter Sattel reference section. Most of the segments
850 (C2 to C7) defined by Menegatti et al. (1998) are recognised in the Argiles à Plicatules
851 Formation.
852 W.F. = Wealden facies, *D. forb* = *Deshayesites forbesi*, Barr. = Barremian, Alb. = Albian.
853 MFS = Maximum Flooding Surface, TST = Transgressive System tract, HST = Highstand
854 system tract.
855
856 Fig. 6. Clay mineralogy of the Argiles à Plicatules Formation (the proportions of chlorite,
857 approximately 5% throughout the formation, are not plotted). *D. forb* = *Deshayesites*
858 *forbesi,* W.F. = Wealden facies.
859 MFS = Maximum Flooding Surface, TST = Transgressive System tract, HST = Highstand
860 system tract.
861

862 Fig. 7. Early Aptian climate trends deduced from $\delta^{13}C_{org}$ and kaolinite content through the
863 Argiles à Plicatules Formation.
864 MFS = Maximum Flooding Surface, TST = Transgressive System tract, HST = Highstand
865 system tract.
866
867
868 Table 1. Rock-Eval data of the studied samples (TOC = Total Organic Carbon, OI = Oxygen
869 index, HI, Hydrogen index).
870
871

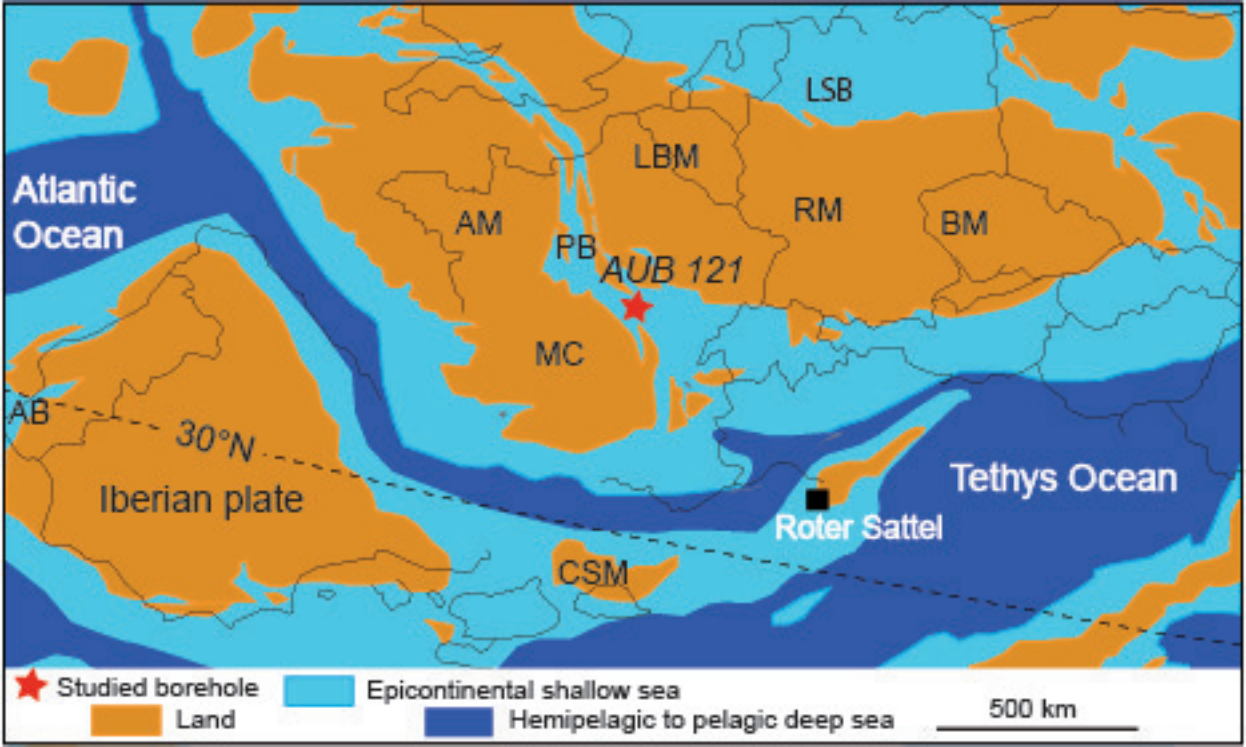
Atlantic Ocean
LSB
LBM
RM
BM
AM
PB
AUB 121
MC
AB
30°N
Iberian plate
Tethys Ocean
Roter Sattel
CSM
Studied borehole
Land
Epicontinental shallow sea
Hemipelagic to pelagic deep sea
500 km

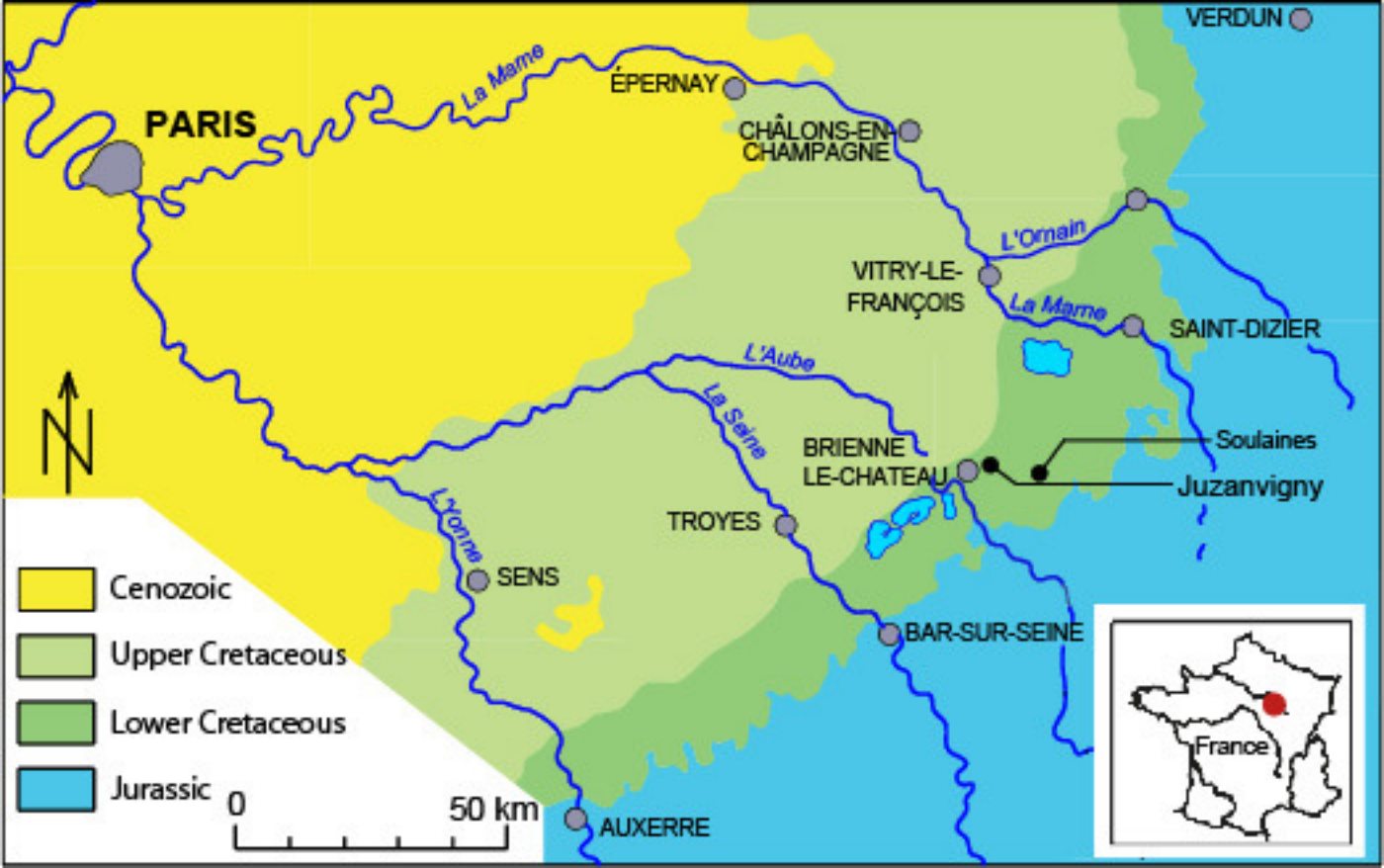
VERDUN
ÉPERNAY
PARIS
La Marne
CHÂLONS-EN-CHAMPAGNE
L'Ornain
VITRY-LE-FRANÇOIS
La Marne
SAINT-DIZIER
L'Aube
La Seine
BRIENNE LE-CHATEAU
Soulaines
Juzanvigny
TROYES
L'Yonne
SENS
BAR-SUR-SEINE
AUXERRE
Cenozoic
Upper Cretaceous
Lower Cretaceous
Jurassic
0
50 km
France

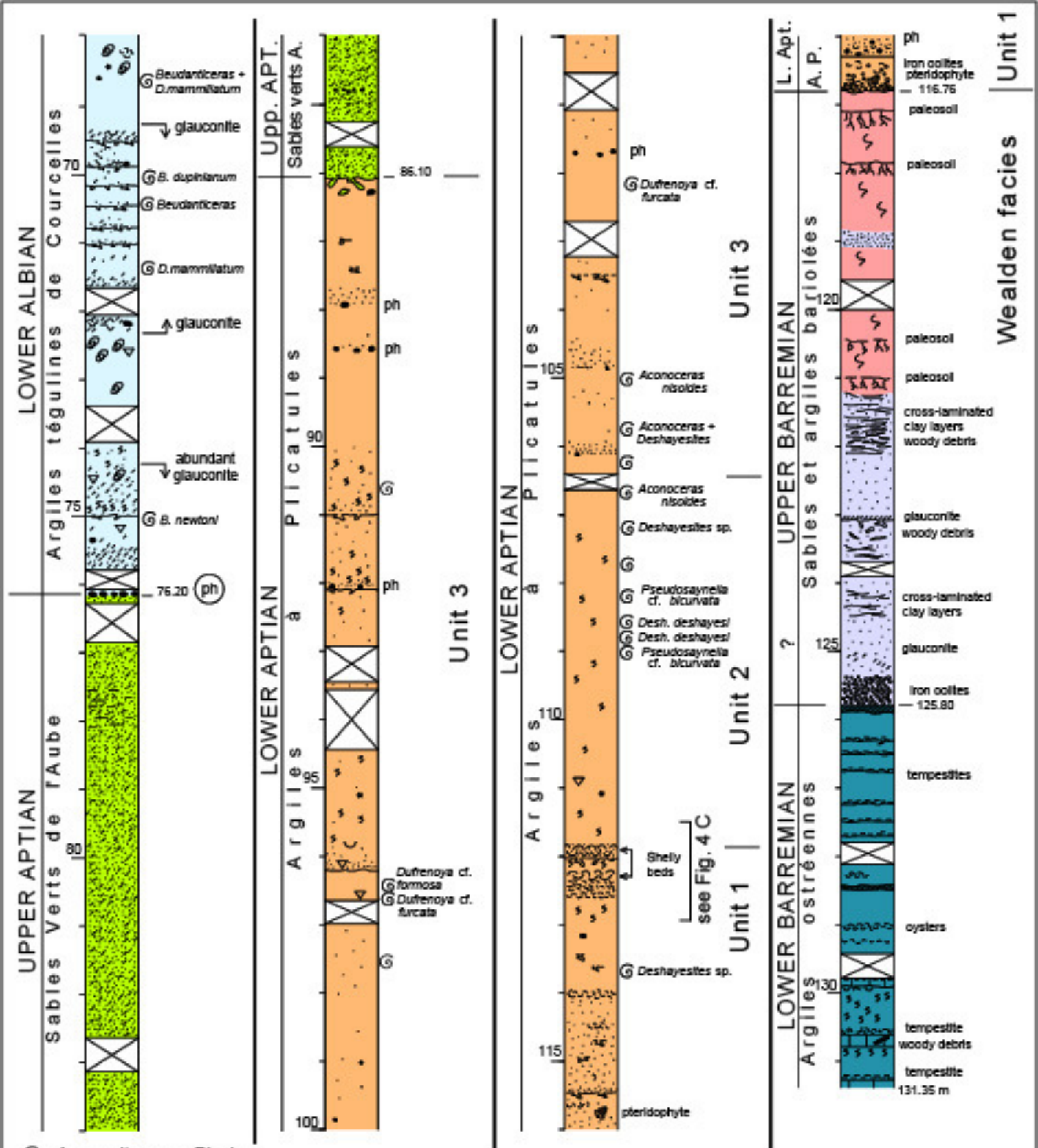
UPPER APTIAN
Sables Verts de l'Aube
LOWER ALBIAN
Argiles tégulines de Courcelles
Beudanticeras + D.mammillatum
glauconite
B. dupinianum
Beudanticeras
D.mammillatum
glauconite
abundant glauconite
B. newtoni
76.20
ph
70
75
80
Upp. APT.
Sables verts A.
LOWER APTIAN
Argiles à Plicatules
86.10
ph
ph
ph
Dufrenoya cf. formosa
Dufrenoya cf. furcata
Unit 3
90
95
100
LOWER APTIAN
Argiles à Plicatules
ph
Dufrenoya cf. furcata
Unit 3
Aconoceras nisoides
Aconoceras + Deshayesites
Aconoceras nisoides
Deshayesites sp.
Pseudosaynella cf. bicurvata
Desh. deshayesi
Desh. deshayesi
Pseudosaynella cf. bicurvata
Unit 2
Shelly beds
see Fig. 4C
Unit 1
Deshayesites sp.
pteridophyte
105
110
115
L. Apt.
A. P.
UPPER BARREMIAN
?
Sables et argiles bariolées
LOWER BARREMIAN
Argiles ostréennes
ph
Iron oolites pteridophyte
116.75
paleosoil
paleosoil
paleosoil
paleosoil
cross-laminated clay layers
woody debris
glauconite
woody debris
cross-laminated clay layers
glauconite
Iron oolites
125.80
tempestites
oysters
tempestite
woody debris
tempestite
131.35 m
120
125
130
Unit 1
Wealden facies
Ammonites
Plicatula
Inoceramids
Bivalves
Chondrites
Thallasinoids
Phosphate nodules = ph
Pyrite

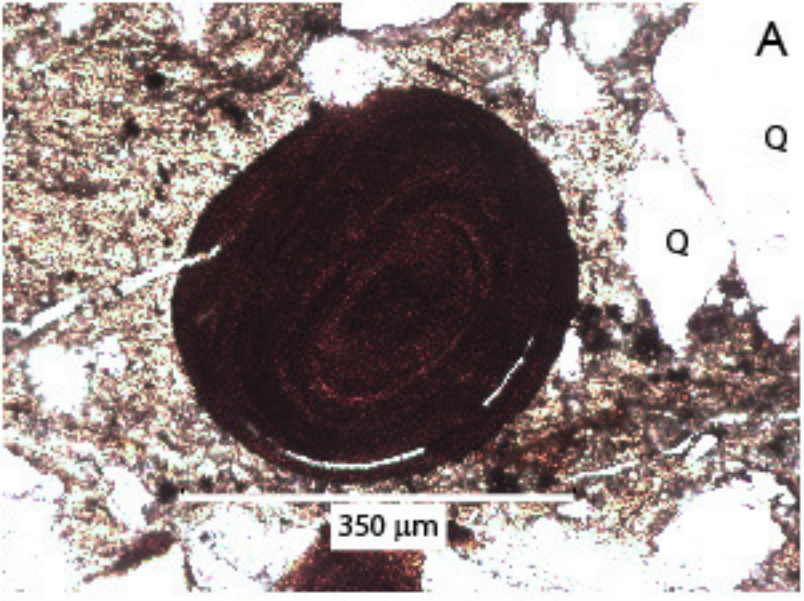
A
Q
Q
350 µm


B
2 cm

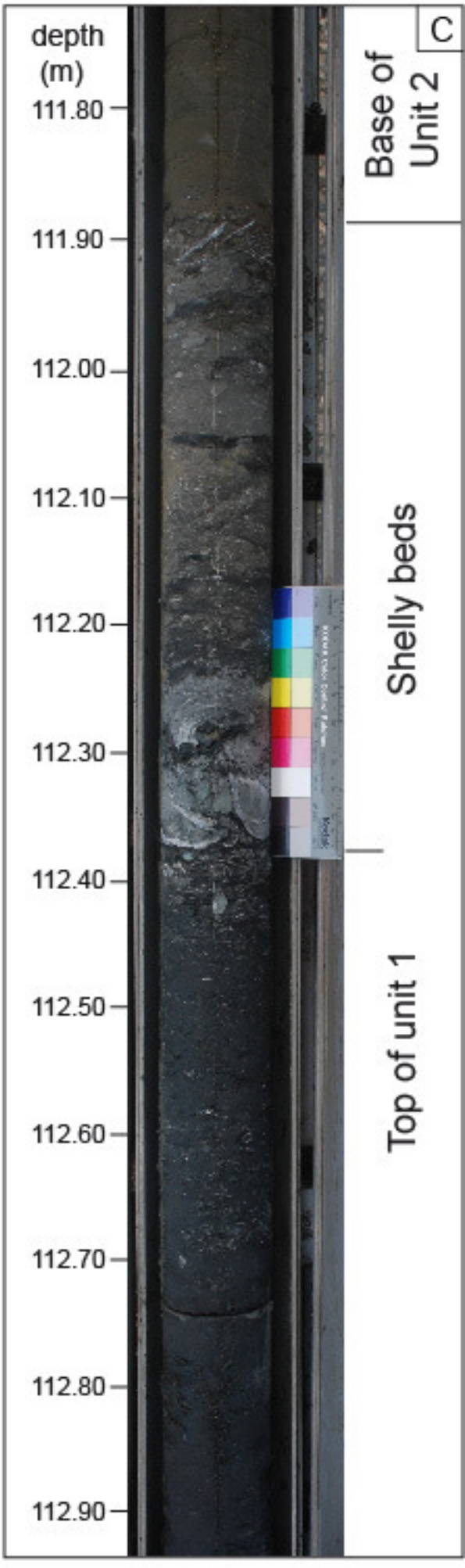
depth
(m)
111.80
111.90
112.00
112.10
112.20
112.30
112.40
112.50
112.60
112.70
112.80
112.90
C
Base of
Unit 2
Shelly beds
Top of unit 1

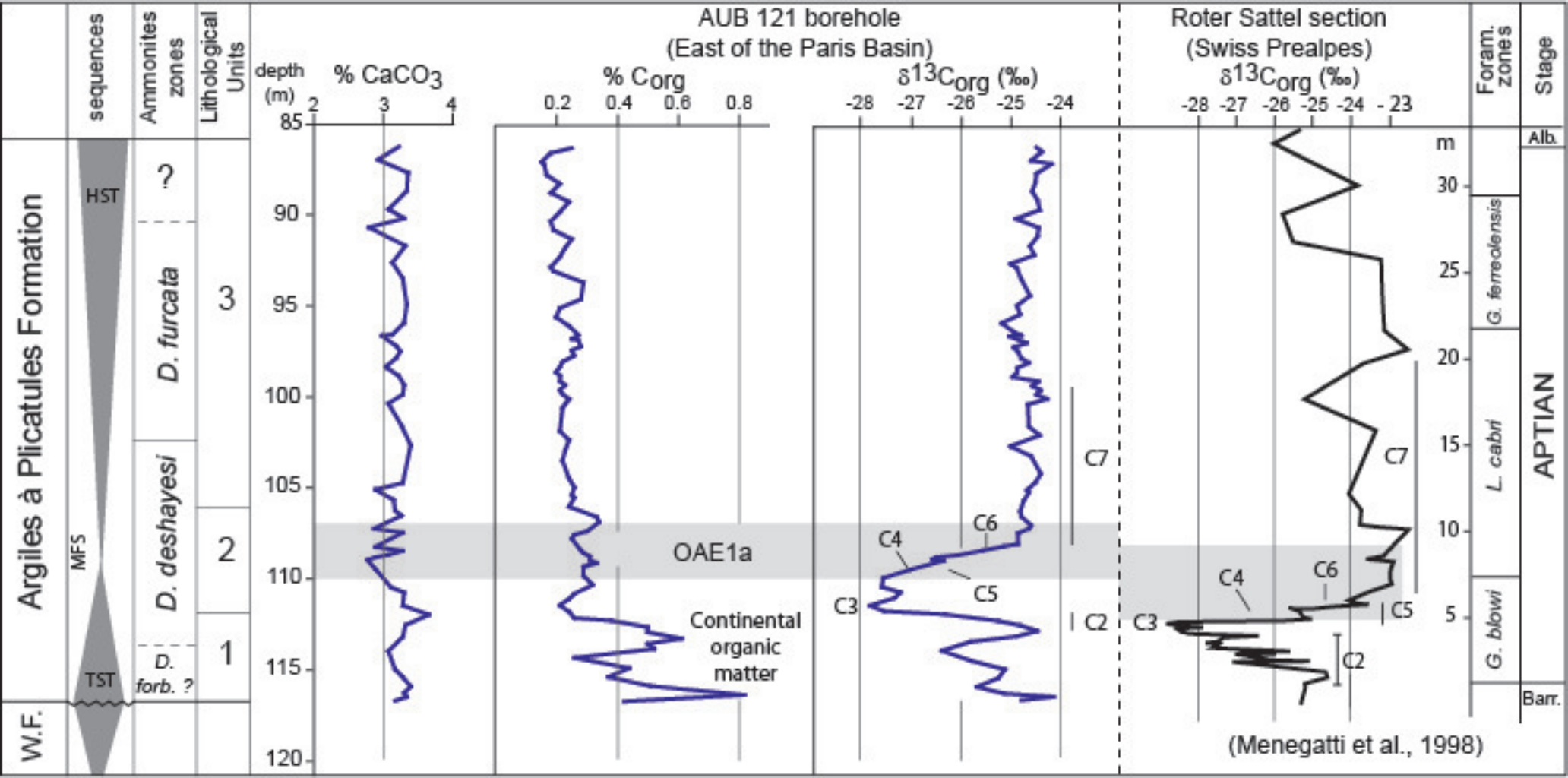
Argiles à Plicatules Formation
W.F.
sequences
HST
MFS
TST
Ammonites zones
?
D. furcata
D. deshayesi
D. forb. ?
Lithological Units
3
2
1
AUB 121 borehole
(East of the Paris Basin)
depth (m)
% CaCO3
% Corg
δ13Corg (‰)
OAE1a
Continental organic matter
C2
C3
C4
C5
C6
C7
Roter Sattel section
(Swiss Prealpes)
δ13Corg (‰)
(Menegatti et al., 1998)
Foram. zones
G. ferreolensis
L. cabri
G. blowi
Stage
Alb.
APTIAN
Barr.

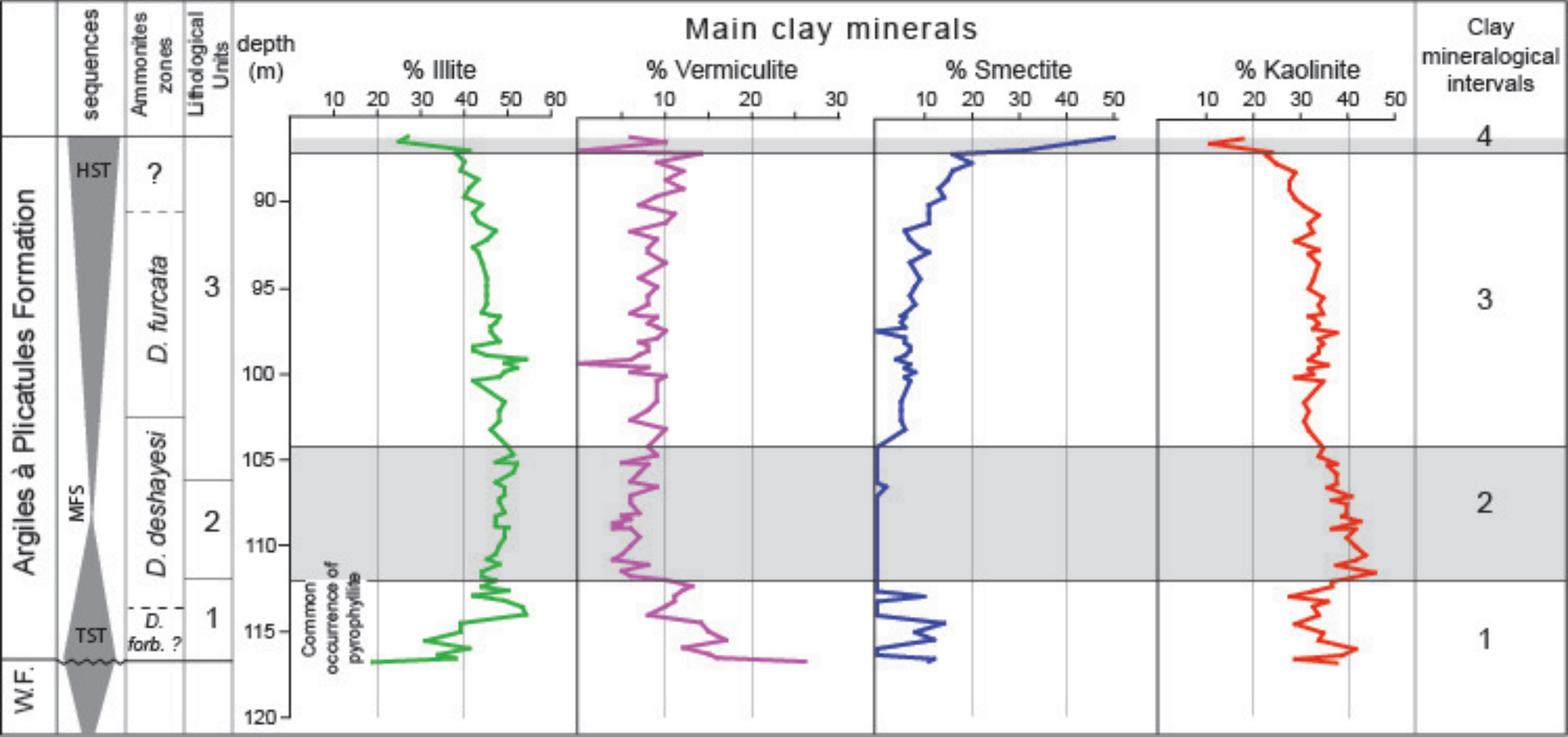
Main clay minerals
sequences
Ammonites zones
Lithological Units
depth (m)
% Illite
% Vermiculite
% Smectite
% Kaolinite
Clay mineralogical intervals
Argiles à Plicatules Formation
HST
MFS
TST
W.F.
?
D. furcata
D. deshayesi
D. forb. ?
3
2
1
Common occurrence of pyrophyllite
4
3
2
1

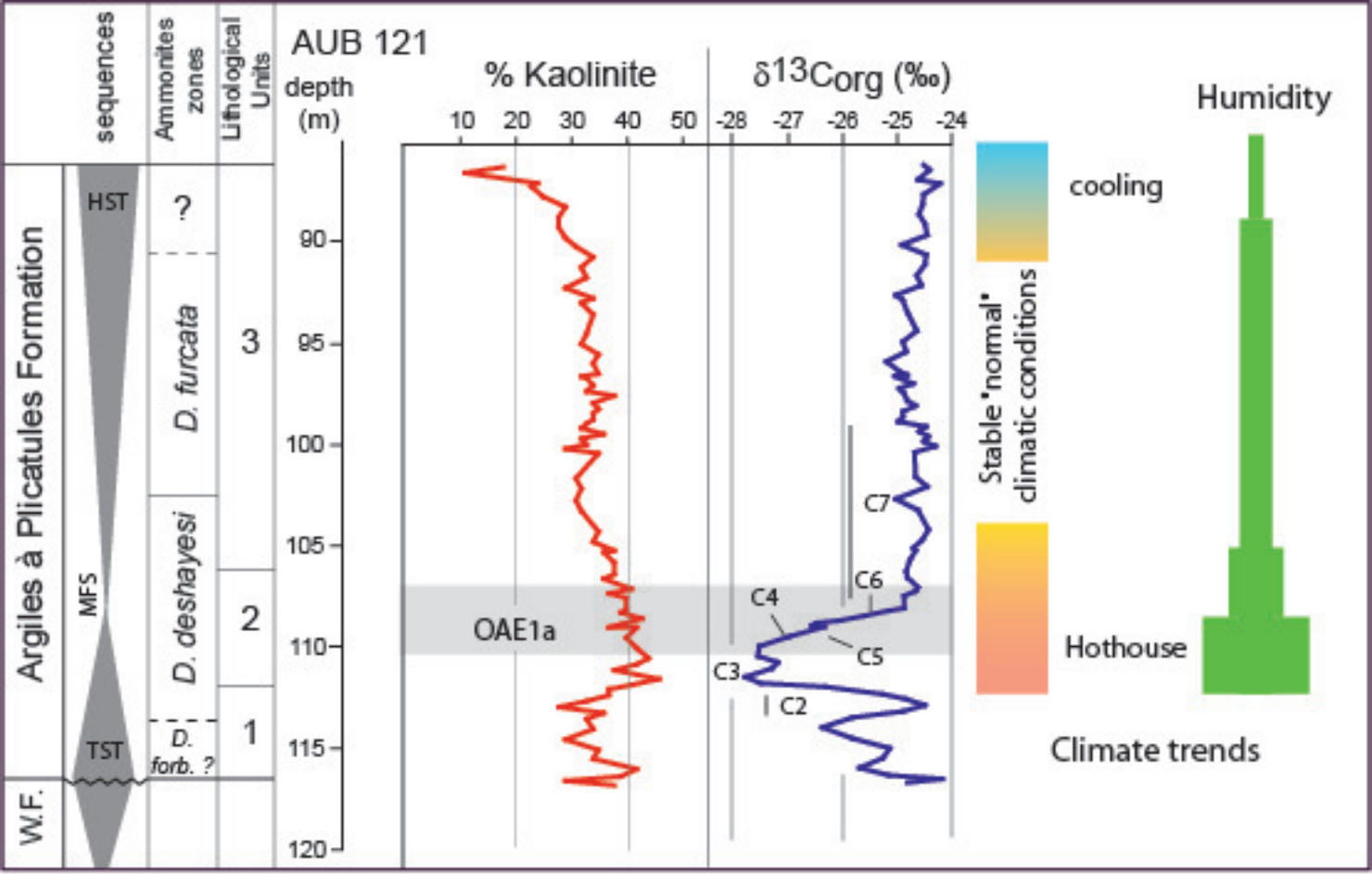
sequences
Ammonites zones
Lithological Units
AUB 121
depth (m)
% Kaolinite
δ13Corg (‰)
Humidity
Argiles à Plicatules Formation
HST
MFS
TST
W.F.
?
D. furcata
D. deshayesi
D. forb. ?
3
2
1
OAE1a
C2
C3
C4
C5
C6
C7
cooling
Stable 'normal' climatic conditions
Hothouse
Climate trends

Sample (depth m)	reliable Tmax (°C)	TOC(%)	HI (mgHC/g TOC)	OI (mgCO2/gTOC
86.45		0.13	54	208
87.12		0.1	70	250
88.15		0.18	67	233
89.15		0.18	33	139
90.15		0.13	54	269
91.15		0.18	39	144
92.15		0.15	33	233
92.90		0.12	52	300
94.42		0.23	43	135
96.42		0.22	45	132
97.00		0.22	45	132
97.50		0.21	33	133
98.13		0.17	53	194
98.63		0.17	53	218
99.13		0.18	44	172
99.63		0.18	36	180
100.13		0.18	44	128
101.10		0.17	41	135
102.10	398	0.21	100	152
103.23		0.17	47	141
104.23		0.2	50	150
105.23		0.19	63	221
107.07		0.21	48	190
108.00		0.16	59	256
110.00	418	0.23	83	148
111.00		0.17	53	229
111.80		0.13	77	277
112.35		0.26	38	92
112.92	384	0.52	56	92
113.52	419	0.44	34	139
114.52b	365	0.38	53	216
114.52a	394	0.4	55	258
115.50		0.42	26	129